Multi-hazard vulnerability modeling: an example of wind and rain vulnerability of mid/high-rise buildings during hurricane events

Zhuoxuan Wei*1,2, Jean-Paul Pinelli1a, Kurtis Gurley2a and Shahid Hamid3a

¹Mechanical and Civil Engineering Department, Florida Institute of Technology, 150 W. University Blvd., Melbourne, Florida, United States ²Engineering School of Sustainable Infrastructure & Environment, University of Florida, Gainesville, Florida, United States ³Department of Finance, College of Business, Florida International University, Modesto A. Maidique Campus, 11200 S.W. 8th Street, Miami, Florida, United States

(Received December 10, 2023, Revised February 27, 2024, Accepted March 3, 2024)

Abstract. Severe natural multi-hazard events can cause damage to infrastructure and economic losses of billions of dollars. The challenges of modeling these losses include dependency between hazards, cause and sequence of loss, and lack of available data. This paper presents and explores multi-hazard loss modeling in the context of the combined wind and rain vulnerability of mid/high-rise buildings during hurricane events. A component-based probabilistic vulnerability model provides the framework to test and contrast two different approaches to treat the multi-hazards: In one, the wind and rain hazard models are both decoupled from the vulnerability model. In the other, only the wind hazard is decoupled, while the rain hazard model is embedded into the vulnerability model. The paper presents the mathematical and conceptual development of each approach, example outputs from each for the same scenario, and a discussion of weaknesses and strengths of each approach.

Keywords: hurricane; mid/high-rise buildings; model decoupling; wind-and-rain vulnerabilities

1. Introduction

Many natural hazard events involve more than one hazard. Multi-hazard events can lead to billions of dollars losses (NOAA 2023). The top three worst years of natural hazards events in the U.S. caused up to \$377, \$256, and \$175 billion dollars (CPI-adjusted) in damage in 2017, 2005, and 2022 respectively, mainly due to tropical cyclones (Miller 2018, NOAA 2023, Smith 2023), which involved wind, surge and flood, and rain. For example, in 2022 there were 17 natural disaster events of which 3 were tropical cyclones causing 65% of the losses or damages.

These multiple hazards can happen concurrently, although their peak intensities might not occur simultaneously. These multiple hazards can be classified as: 1) concurrent and independent, for example, earthquake and hurricane happening simultaneously; 2) concurrent and correlated. For example, dual-hazard hail and tornadic winds in thunderstorms; or tri-hazard high winds, wind-driven rain, and either inland flooding or coastal storm surge in hurricanes (Li et al. 2012, NOAA 2023); or high wind and ice hazards in winter storms (Mahmoudi et al. 2021). Multi-hazards can also be cascading rather than concurrent, occurring in hazard chains, for example, earthquake-blast chain (Francioli et al. 2023), earthquake and tsunami; earthquake and fire; rainfall and landslide.

Modeling losses from multi-hazard events present many

_

sequencing issues (Zaghi et al. 2016). At the hazard stage, for hurricane exposed infrastructure, wind, rain, surge, waves and inland flooding vary in time and space, and the duration of the overlap may directly influence multi-hazard effects (Nofal et al. 2021). Heavy rainfall may affect buildings in the hurricane's track from coastline to inland (Matyas 2010). At the vulnerability stage, different hazards commonly damage different components of the same structure. Wind damages the building exterior systems and appurtenant, allowing rainwater ingress to damage interior components and contents (Lu et al. 2021, Pita et al. 2012, Sim et al. 2020). Storm surge, wave, and flood can cause both structural and interior damage and even collapse buildings (Baradaranshoraka et al. 2019, Kennedy et al. 2020, Paleo-Torres et al. 2020, Tomiczek et al. 2014). A cooccurrence of storm surge and riverine flooding may intensify the inundation effect. At the design strategy stage, current design codes are strength-based and generally consider multi-hazard interaction only through load combinations and load factors, which usually do not account for possible changes in the characteristics of structures because of individual hazards. Petrini et al. (2020) summarized the practical issues arising when the design of bridges in a multi-hazard framework. Similarly, (Ciabattoni et al. 2024) proposed a unified design framework for the design of tall buildings subjected to both earthquakes and high winds. These design issues are especially relevant in the context of a performance-based design scenario, but this paper focuses on catastrophe modeling over large portfolios of buildings.

challenges related to the hazards themselves, their

interaction with the built environment, and timing and

Catastrophe (cat) models are developed to project the

ISSN: 1226-6116 (Print), 1598-6225 (Online)

^{*}Corresponding author, Ph.D. Candidate E-mail: weiz2018@my.fit.edu

^aPh.D. Professor

natural hazard induced damage to infrastructure. Typically, cat models include four main components (Pita et al. 2013): a component which models the hazard (hazard model); a component that categorizes the building exposure into generic building classes (BC); a component which models the effects of the hazard on the exposure to define vulnerability functions for each building class (vulnerability model); and a component which utilizes outputs from the hazard, exposure and vulnerability components to quantify the actuarial risk in terms of economic damage and insured losses (actuarial model). Examples of cat models include (Barbato et al. 2013, Biasi et al. 2017, Bhandari et al. 2018, Chian 2016, Dong 2002, Hatzikyriakou and Lin 2016, Henderson and Ginger 2007, Ma et al. 2021, Michel-Kerjan et al. 2013, RMS (Risk Management Solutions), 2021, Wang *et al.* 2021).

To project hazard intensities researchers typically develop a separate model for each hazard. For example, separate models for hurricane winds, surge, and inland flood (Dietrich et al. 2012, Nofal et al. 2021, Powell et al. 2010). In that context, it is difficult when employing these models in a multi-hazard framework to capture the dependency and/or correlation between hazards. In addition, field data might be more prevalent for one hazard than the other, e.g., more wind data available but no rain data (Knabb et al. 2005, 2006), which can complicate the validation of different hazard models. Moreover, modeling interaction between multiple hazards might computationally intensive (Borgonovo et al. 2012, Geist et al. 2009, Luger and Harris 2010, Tilloy et al. 2019).

Traditionally, cat modelers have approached multihazard loss modeling by projecting losses from one hazard at a time, and then combining the results into overall losses via empirical relationships (Baradaranshoraka *et al.* 2017, Ming *et al.* 2015, Nofal and Lindt 2020). However, there is a dearth of data available to validate multi-hazard model loss outputs since insurance claim data do not in general distinguish between causes of loss in a multi-hazard cause of loss scenario.

This paper illustrates two different approaches to treat the multi-hazards and discusses weaknesses and strengths of these two approaches. In the first approach, the different hazard models are decoupled from the vulnerability model, insuring independence of the hazard and vulnerability models. In the second approach, the hazards are classified as primary and secondary, and only the primary hazard model is decoupled, while the secondary hazard model is embedded into the vulnerability model. Section 2 presents the two proposed approaches for multi-hazard loss modeling. Section 3 briefly describes a vulnerability model developed by the authors. Section 4 introduces the hazard model and the probability distribution of hazard intensities derived from the hazard model. The vulnerability model in section 3 is then tested with the proposed decoupled and coupled approaches. Section 5 and 6 illustrate the implementation and outputs of the two approaches. Section 7 presents the pros and cons and relationship between outputs of the two approaches respectively.

2. Different approaches for multi-hazard vulnerability modeling

2.1 Single hazard case

Most probabilistic vulnerability models employ a Monte-Carlo (MC) simulation engine. In the case of a single-hazard event, in general the hazard intensity is discretized over a pre-defined range and intervals, and the vulnerability being produced via MC is conditional upon these hazard intensities. Thus, over a series of discrete and defined hazard intensities, the MC program produces a large number of samples of building and contents damage, where the random variables that vary between samples may be any or a combination of the building component capacities, interior damage propagation, and conversion from physical damage to repair cost. This repair cost in ratio with the building value is the damage ratio, and is the typical output presented as dependent on (conditional upon) hazard intensity. The results of the MC simulations are collected in a vulnerability matrix, with samples of damage ratio down the rows and discretized hazard intensities along the columns. A histogram of any column provides a probability mass function of damage ratio as a function of the discrete hazard intensity assigned to that column. Averaging through each column produces the vector pair of mean damage ratio and hazard intensity which can be plotted as a vulnerability curve.

The specific content of the vulnerability matrix and shape of the vulnerability curve are of course strongly dependent upon the nature of the infrastructure or building class they represent. Consider vulnerability (matrix and curve) conditional upon the peak wind speed in a hurricane hazard. In Florida, the vulnerability of a 1970's constructed single family wood frame residential home would differ considerably from a 2023 constructed single family reinforced masonry residential home, due to choice of materials, aging, and the advancement of load path requirements in building codes. Thus, projecting losses over a region due to a hazard with a large geographic footprint (e.g., hurricane) requires the generation of a library of many vulnerability matrices for different building classes to properly capture the breadth of the building inventory being impacted.

As an expression of damage probability conditional upon a given hazard intensity, the vulnerability matrix (or curve) has nothing to say about the likelihood of any specific hazard intensity in single hazard cases. This is the role of the hazard model. For example, a hurricane wind hazard model is employed to generate the geometrically varying time history of wind speed and wind direction of a hurricane over its life. The hazard and vulnerability models are combined in the actuarial model for either the simulation of a real historical hurricane event (scenario simulation) or the creation of a fictitious event that is designed to behave within the stochastic bounds of the record of real past real events (stochastic simulation). In the stochastic mode, a given portfolio of exposure is subjected to thousands of fictitious simulated hurricanes, where each simulated hurricane is treated as a fictitious scenario.

Hazard model outputs are employed to inform the probability of the conditional (independent) hazard variable in the vulnerability matrix or curve. In a scenario analysis, the combined hazard and vulnerability models will project losses from past hurricanes, thus providing a means of validation by comparing projections against real insurance claims data from those events. In a stochastic analysis, the hazard and vulnerability models can be used to project average annual losses from hurricane wind damage, aggregated by region or stratified further by structure type (Hamid *et al.* 2011, Pinelli *et al.* 2011, Pita *et al.* 2015, Pita *et al.* 2013).

2.2 Multi-hazard case: hazard and vulnerability decoupling

This single-hazard strategy can be expanded to the case of multiple simultaneous hazard events, e.g., hurricane winds and rain. In the so-called decoupling approach, the various hazard intensities are discretized over pre-defined ranges and intervals, and the vulnerability being produced via MC is conditional upon combinations of these hazard intensities. The results of the MC simulations are collected in multi-dimensional vulnerability tensors, where each cell yields probabilities of damage given combined hazard intensities. A histogram of any column provides a probability mass function of damage ratio as a function of the combined discrete hazard intensities assigned to that column. Averaging through each column produces the combinations of mean damage ratio and hazard intensities which can be plotted as a vulnerability surface, for the case of two hazards. The vulnerability model outputs are conditioned upon discretized hazard intensities, and are therefore independent of the hazard model(s), in the same way than for the single hazard case.

This decoupling of the multiple hazard model(s) and vulnerability model have advantages and disadvantages. First, the multi-hazard vulnerability functions require that either different hazard models, or an integrated multi-hazard model provide estimates of all hazard intensities at each location of the exposure. In that case, for each scenario analysis, either real or fictitious (in the case of a stochastic analysis), mean values of damage are assigned based on the corresponding combined hazard intensities. Section 3 below shows that in a decouple model, separate vulnerability curves conditional on each hazard can be developed. The independence of the vulnerability model and hazard model(s) makes it easy to test the influences of different hazard model(s) on the projected insured losses. The decoupling approach is computationally intensive for both hazard modeling and the vulnerability modeling. On the hazard side it requires prediction of all the hazard intensities at every location. On the vulnerability side it requires a large number of simulations for all combinations of hazard intensities.

2.3 multi-hazard case: hazard and vulnerability coupling

A different approach for multi-hazard vulnerability

modeling defines one hazard as the primary (independent) hazard and the others as secondary hazards. In cases where there is a correlation between primary and secondary hazards, probability distribution functions (PDFs) of secondary hazard intensities conditional on primary hazard intensities can be developed. An example will be provided in section 4. This strategy mimics the single-hazard implementation, where the primary hazard intensity is discretized over a pre-defined range and intervals, and the vulnerability being produced via MC is conditional upon these primary hazard intensities. For each MC simulation, the secondary hazard intensity is not discretized. Instead, it is sampled from its PDF as a function of the assigned primary hazard intensity, and is therefore embedded in the vulnerability model. Results are vulnerability matrices which yield probabilities of damage conditional on the primary hazard intensity. The coupled secondary hazard and vulnerability model is essentially a one-hazard model, which is transparent to the secondary hazard.

The advantages and disadvantages of this coupling approach are the opposites to those of the decoupling approach. First, the primary-hazard vulnerability functions require only primary-hazard intensities at each location of the exposure to estimate the damage. In that case, for each scenario analysis, either real or fictitious (in the case of a stochastic analysis), mean values of damage are assigned based on the corresponding primary hazard intensities. The dependence of the vulnerability model on the secondary hazard model makes it difficult to test the influences of alternative secondary hazard modes on the projected insured losses. The approach can produce vulnerability curves dependent on the primary-hazard only. The coupling approach is computationally less intensive for both hazard modeling and the vulnerability modeling. On the hazard side it requires prediction of only the primary hazard intensities at every location. On the vulnerability side it does not require simulations for all combinations of hazard intensities.

3. Mid/high-rise hurricane wind and rain vulnerability model

The paper illustrates the two vulnerability modeling approaches described above for the case of mid/high-rise buildings subjected to hurricanes. With funding from the Florida Office of Insurance Regulation (OIR) and the Wind Hazard and Infrastructure Performance Center (WHIP-C), the authors developed a component-based probabilistic vulnerability model to predict wind and rain vulnerability of mid/high-rise buildings (MHRB) during hurricane events. This model referred to as the WHIP-MHRB categorizes the MHRB into different BC's, and for each BC, the model projects interior and exterior building damage, contents damage, and it also includes a module, the WHIP-TRE, which projects recovery time and time related expenses (TRE). Both the WHIP-MHRB and the WHIP-TRE are described in detail in companion papers (Wei et al. 2024, Wei et al. 2024). In this case, the multiple hazards are the wind and the wind-driven rain. The wind hazard is the

primary hazard, and its intensity is the 3-sec maximum peak gust wind speed at 10 meters height over actual terrain (WS_{max}), and the height of accumulated wind-driven rain from start to end of the storm at a height of 10 m (WDR_{h10}), is the secondary hazard intensity. Although there is no causality between WS_{max} and WDR_{h10}, we shall see in the next section that there is a correlation between the two, and probability distribution functions of WDR_{h10} conditional on WS_{max} can be derived.

MHRB are engineered structures and therefore highly resistant to wind induced structural damage. For that reason, the Florida Public Hurricane Loss Model (FPHLM), from which the WHIP-MHRB is derived, only considers damage to exterior openings (windows, doors, and sliders) and water ingress via a component approach (Pita *et al.* 2016). In the WHIP-MHRB model, the authors took the FPHLM component approach one step further to capture the physics of wind-driven rainwater ingress, distribution and propagation to produce estimates of hurricane damage to both interior and contents in MHRB. Water may ingress absent any physical damage (e.g., an undamaged window can leak), through installation, product, or maintenance defect, and through the breaches of the envelope due to wind or debris impact.

At the heart of the WHIP-MHRB model is a MC simulation engine, which conducts large numbers (n) of simulations (in this paper n=2000) for different combinations of WS_{max} , wind direction, and WDR_{h10} . WS_{max} is discretized into 41 intervals from 22.35 m/s (50 mph) to 111.76 m/s (250 mph) with a width of 2.26 m/s (5 mph). The wind direction is selected from 0° to 315° in 45° increments. WDR_{h10} is either discretized into 20 intervals from 0 m to 2.54 m with a length of 0.13 m in the decoupling approach, or sampled from its pdf conditional on WS_{max} as described in section 4 (coupling approach). The result of the simulations are distributions of damage to the exterior, interior, and contents components of the building, with subsequent recovery times and TRE. These damage simulations are then transformed into vulnerability tensors and matrices, and their respective vulnerability surfaces and curves.

In the following sections, the authors illustrate the details of the decoupling and coupling approaches within the framework of the WHIP-MHRB.

4. Hazard model

For muti-hazards, the same hazard model could produce the estimates of both the primary and secondary hazard intensities, in this case, WS_{max} and WDR_{h10} or different models can independently produce the primary and secondary hazard intensities. Although the first case is preferable, especially if a decoupled vulnerability model is used (described in section 5), the FPHLM v8.2 (FPHLM 2022) and the WHIP-MHRB hazard models follow the second case strategy. The wind model was developed initially by (Powell *et al.* 2005) without a rain component. Later, Pita *et al.* (2012) performed an independent study on the estimation of WDR_{h10} during hurricane events via

simulation of a large number of synthetic hurricanes. For each of these hurricanes, the radially averaged rain rate and wind speed distribution (assuming that tangential wind is the full wind speed) are estimated based on models by (Holland 1980, Marks *et al.* 1993), respectively. A number of recording stations are placed uniformly across each synthetic hurricane at a given distance from the coast. The simulation records the time history of rain rate and wind speed at each station for all synthetic hurricanes resulting in probability distribution functions of WDR_{h10} conditional on WS_{max}, and vice-versa.

$$p_1(i,j) = P^H (WDR_{h10} = wdr_j | WS_{max} = ws_i) = \frac{n_{ij}^H}{n_i^H}$$
 (1)

$$p_2(i,j) = P^H(WS_{max} = ws_i|WDR_{h10} = wdr_j) = \frac{n_{ij}^H}{n_i^H}$$
 (2)

 $P^H(A|B)$ = the conditional probability distribution function derived from the rain hazard model (hence the superscript H), e.g., $P^H(WDR_{h10} = wdr_j|WS_{max} = ws_i)$ is the probability that WDR_{h10} is in the j-th WDR_{h10} interval given that the WS_{max} is the i-th WS_{max} interval.

 n_{ij}^H = the number of simulations instances in the i-th WS_{max} interval and j-th WDR_{h10} interval simultaneously.

 n_i^H = the number of simulations instances in the i-th WS_{max} interval.

5. Hazards and vulnerability models decoupling in the WHIP-MHRB model

In the decoupling approach (Fig. 1(a)) the MC simulation vulnerability engine treats both WS_{max} and WDR_{h10} as deterministic variables. For each wind direction, for every combination of WS_{max}, WDR_{h10}, a number n of simulation is carried out, which produce building and contents damage ratios (DR) and recovery times (Treco). For each BC, the results of the simulations translate into building, contents, and recovery times vulnerability tensors and vulnerability surfaces where, the expected damage ratios are conditional on both WS_{max} and WDR_{h10}, $\overline{DR_{BC}}$ (WS_{max}, WDR_{h10}).

Outputs of the WHIP-MHRB Model include 3D vulnerability tensors, vulnerability surfaces, vulnerability matrices and curves which are detailed in the following sections. The Eqs. (3)-(11) below are developed to express damage ratios, but they can also be adapted to express recovery times and TRE.

5.1 3D vulnerability tensor and vulnerability surface

For each BC, the combinations of WS_{max} , WDR_{h10} , and damage ratios (DR), directly result in a 3D vulnerability tensor (Fig. 2), V_1 , with a dimension of $250 \times 41 \times 20$ representing 250 equal DR intervals from 0 to 100%, 41 WS_{max} intervals, and 20 WDR_{h10} intervals. V_1 is independent of the distributions of WS_{max} and WDR_{h10} . Each cell of V_1 is a conditional probability of damage from Eq. (3).

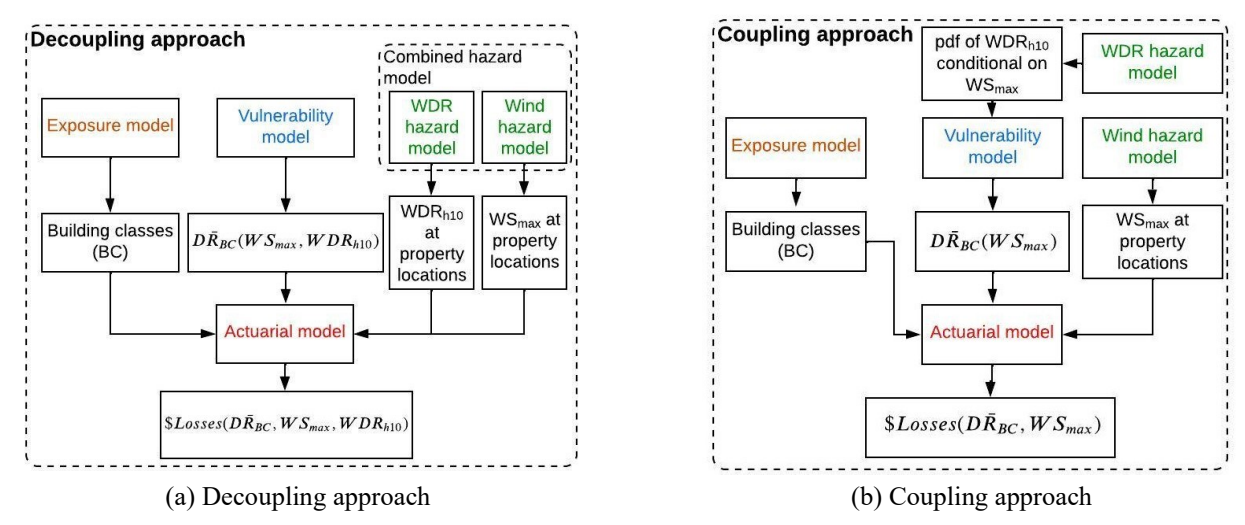


Fig. 1 Difference between decoupling approach and coupling approaches

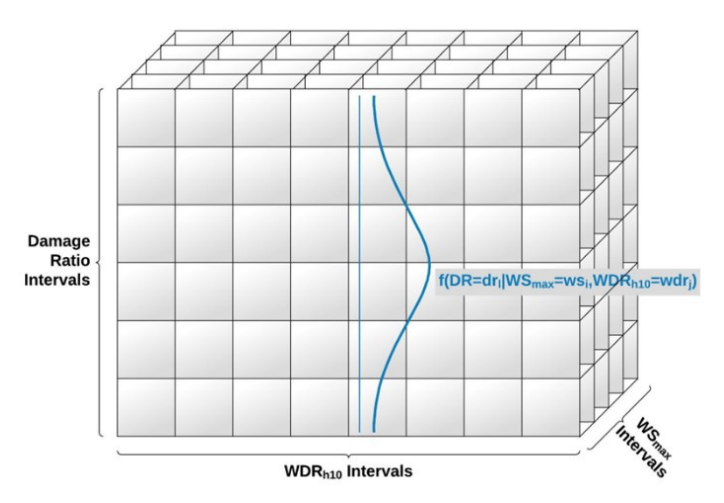


Fig. 2 Schematic of 3D vulnerability tensor

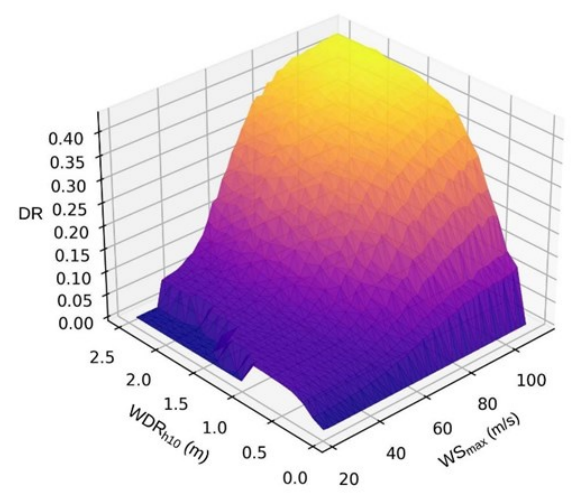


Fig. 3 Vulnerability surface for BC: open_U6_S6_NSD_IR_C

$$\begin{split} V_1(m,i,j) &= P \Big(DR = dr_m | WS_{max} = ws_i, WDR_{h10} = wdr_j \Big) \\ &= \frac{n_{mij}}{n_{ij}} \end{split} \tag{3}$$

 n_{mij} = the number of simulation data points with DR in the m-th DR interval, WS_{max} in the i-th WS_{max} interval, and WDR_{h10} in the j-th WDR_{h10} interval.

 n_{ij} = the number of simulation data points with WS_{max}

in the i-th WS_{max} interval, and WDR_{h10} in the j-th WDR_{h10} interval.

The vulnerability surface gives the mean damage ratio given a certain combination of WS_{max} and WDR_{h10} calculated with Eq. (4). Fig. 3 is an example of vulnerability surface showing the mean building DR for a building class with open layout, 6 stories and 6 apartments per story, without sliding balcony door, impact resistant glass, and carpet floor (open U6 S6 NSD IR C).

$$\overline{DR}(WS_{max} = ws_i, WDR_{h10} = wdr_j)$$

$$= \sum_{\substack{m=1 \\ m_{max}}} dr_m \cdot V_1(m, i, j)$$

$$= \sum_{\substack{m=1 \\ m_{max}}} dr_m \cdot \frac{n_{mij}}{n_{ij}}$$
(4)

5.2 Vulnerability matrices and vulnerability curves

In many cases, only one hazard intensity, WS_{max} or WDR_{h10}, at a particular building location is provided, or the distribution of damage with respect to one hazard only is required. In that case, it is necessary to reduce the vulnerability tensor V₁ with probabilities conditional on two hazard intensities to a vulnerability matrix probabilities conditional on only one, WS_{max} or WDR_{h10}. The resulting vulnerability matrices, V2, conditional on WS_{max} and V_3 , conditional on WDR_{h10} are derived from V_1 thanks to Eqs. (5)-(6). In these matrices, each column provides the pdf of DR conditional on WS_{max} or WDR_{h10} (Fig. 4). In these equations, p_1 and p_2 are the pdf of WDR_{h10} conditional on WSmax and WSmax conditional on WDRh10 derived from the hazard model (Eqs. (1)-(2)). Therefore, in these vulnerability matrices we lose the independence between hazard and vulnerability models.

$$V_{2}(m,i) = P(DR = dr_{m}|WS_{max} = ws_{i})$$

$$= \sum_{\substack{j=1 \ j_{max}}} [V_{1}(m,i,j) \cdot p_{1}(i,j)]$$

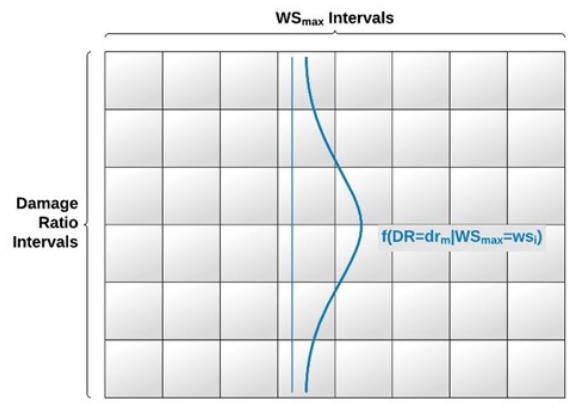
$$= \sum_{\substack{i=1 \ j_{max}}} \left(\frac{n_{mij}}{n_{ij}} \cdot \frac{n_{ij}^{H}}{n_{i}^{H}}\right)$$
(5)

$$V_{3}(m,j) = P(DR = dr_{m}|WDR_{h10} = wdr_{j})$$

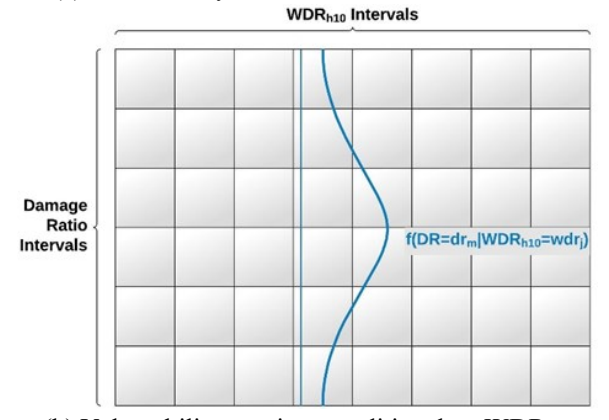
$$= \sum_{i=1}^{l_{max}} [V_{1}(m,i,j) \cdot p_{2}(i,j)]$$

$$= \sum_{i=1}^{l_{max}} \left(\frac{n_{mij}}{n_{ij}} \cdot \frac{n_{ij}^{H}}{n_{j}^{H}}\right)$$
(6)

The vulnerability curves provide the mean damage ratio given a certain WS_{max} or WDR_{h10} calculated with Eqs. (7)-(8) respectively. Fig. 5 shows the WS_{max} and WDR_{h10} vulnerability curves for the same BC used for Fig. 3.



(a) Vulnerability matrices conditional on WS_{max}



(b) Vulnerability matrices conditional on WDR_{h10} Fig. 4 Vulnerability matrices conditional on: WS_{max} and

$$\overline{DR}(WS_{max} = ws_i) = \sum_{m=1}^{m_{max}} dr_m \cdot V_2(m, i)$$

$$= \sum_{m=1}^{m_{max}} dr_m \cdot \sum_{i=1}^{j_{max}} \left(\frac{n_{mij}}{n_{ij}} \cdot \frac{n_{ij}^H}{n_i^H}\right) \tag{7}$$

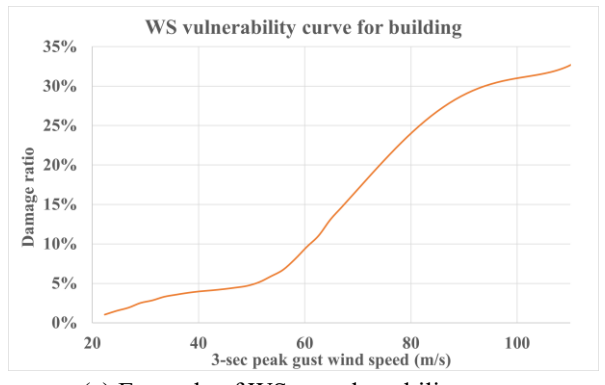
$$\overline{DR}(WDR_{h10} = wdr_j) = \sum_{m=1}^{m_{max}} dr_m \cdot V_3(m,j)$$

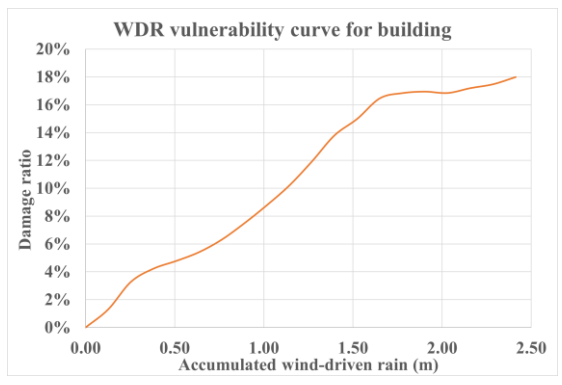
$$= \sum_{m=1}^{m_{max}} dr_m \cdot \sum_{i=1}^{i_{max}} \left(\frac{n_{mij}}{n_{ij}} \cdot \frac{n_{ij}^H}{n_j^H} \right) \tag{8}$$

5.3 Insured losses

 WDR_{h10}

In the actuarial model, each building in an insurance portfolio is assigned a building class BC, with its corresponding vulnerability surface $\overline{DR_{BC}}$, and the combination of wind hazard intensity WS_{max}, and WDR hazard intensity WDR_{h10}, results in a mean damage ratio. Deductible and limit transform the resulting damage into a mean insured loss, $\overline{\$L_k}$, for each property in a portfolio, which is:





(a) Example of WS_{max} vulnerability curve

(b) Example of WDR_{h10} vulnerability curve

Fig. 5 WS_{max} and WDR_{h10} vulnerability curves for BC: open U6 S6 NSD IR C

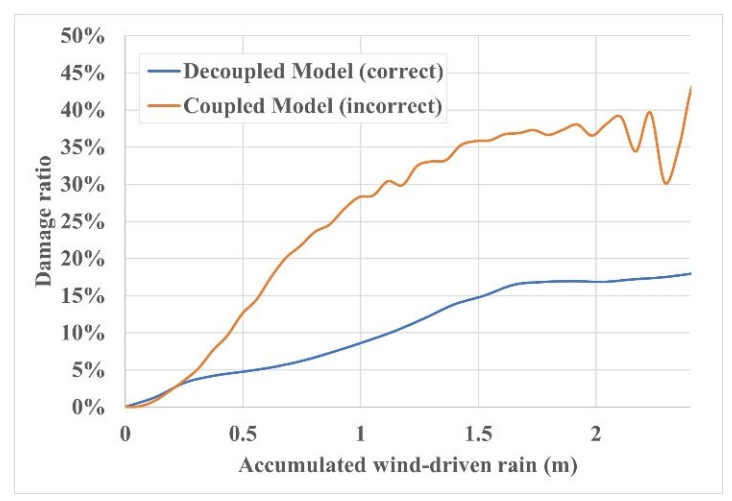


Fig. 6 Comparison of WDR_{h10} vulnerability curves from decoupled model (correct) and coupled model (incorrect)

$$\overline{\$L_k} = \max\left(0, \left(\overline{DR_{BC}}(WS_{max} = ws_i, WDR_{h10} - wdr_i\right) \cdot \$V_k - D_k\right)\right) \le Limit_k$$
(9)

 V_k = the building value. D_k = the insurance deductible.

 $Limit_k$ = the insurance limit.

With the decoupled vulnerability model, the actuarial model can take advantage of intensity information on both WS and WDR at the location of the property, resulting in potentially more accurate estimate of the loss.

If only a single hazard intensity (either wind WS_{max} or rain WDR_{h10}) is available at the location of the property, the mean loss based on either one of these hazard intensities can still be computed from the vulnerability matrices V_2 or V_3 and their corresponding vulnerability curves as follows.

$$\overline{\$L_k} = \max(0, (\overline{DR_{BC}}(WS_{max} = ws_i) \cdot \$V_k - D_k))$$

$$\leq Limit_k$$
(10)

$$\overline{\$L_k} = \max\left(0, \left(\overline{DR_{BC}}(WDR_{h10} = wdr_j) \cdot \$V_k - D_k\right)\right)$$

$$\leq Limit_k$$
(11)

In this case, for example in Eq. (10) the pdf's of WDR are embedded in the vulnerability model, and the estimate of the loss does not consider the local intensities of WDR.

6. Hazards and vulnerability models coupling in the WHIP-MHRB model

In the coupling approach (Fig 1(b)) the MC simulation vulnerability engine treats WS_{max} as a deterministic variable, while for each simulation WDR_{h10} is sampled from its pdf conditional on WS_{max}. In this case the rain hazard model is embedded in the vulnerability model. For each combination of wind direction and WS_{max}, a number n of simulation is carried out, which produce building and contents damage ratios (DR) and recovery times (Treco). For each BC, the results of the simulations translate into building, contents, and recovery times vulnerability matrices. The vulnerability curves give the expected damage ratios $\overline{DR_{BC}}(WS_{max})$ conditional on WS_{max}, as in a one-hazard case. The coupling approach is the default approach in both the original FPHLM (Johnson et al. 2018, Pita et al. 2012, Pita et al. 2016) and the WHIP-MHRB (including its WHIP-TRE component).

The following sub-sections describe the outputs of the WHIP-MHRB Model, which include vulnerability matrices

and curves. The Eqs. (12)-(14) are developed to express damage ratios, but they can also be adapted to express recovery times and TRE.

6.1 Vulnerability matrices and curves

For each BC, the outputs of the coupled WHIP-MHRB model are vulnerability matrices, V_2 , where each cell represents the probabilities of damage conditional on only WS_{max} (Eq. (12)). In these matrices, each column provides the pdf of DR conditional on WS_{max} (Fig. 4(a)).

$$V_2(m, i) = P(DR = dr_m | WS_{max} = ws_i) = \frac{n_{mi}}{n_i}$$
 (12)

 n_{mi} = the number of data points of having the m-th DR interval, and i-th WS_{max} interval from vulnerability model.

 n_i = the number of data points of having the i-th WS_{max} interval from vulnerability model.

The vulnerability curves give mean damage ratio as a function of WS_{max} (Eq. (13)).

$$\overline{DR}(WS_{max} = ws_i) = \sum_{\substack{m=1\\m_{max}}}^{m_{max}} dr_m \cdot V_2(m, i)$$

$$= \sum_{\substack{m=1\\m=1}}^{m_{max}} dr_m \cdot \frac{n_{mi}}{n_i}$$
(13)

The vulnerability matrix from Eq. (12) and the vulnerability curve from Eq. (13) are theoretically the same as the ones from Eqs. (5) and (7), provided that the same hazard model yielding the same pdf's of secondary hazard conditional on primary hazard $(p_1 \text{ Eq. } (1))$ are used in both models.

6.2 Limitations of the coupling approach

In the coupling approach, where WDR $_{h10}$ is sampled from a pdf instead of being treated as an independent deterministic variable, each simulation results in combinations of WS $_{max}$, WDR $_{h10}$, and DR. Therefore, a 3D vulnerability tensor V $_1$ could also be derived from the simulations, where theoretically the cells would represent the probabilities of DR conditional on both WS $_{max}$ and WDR $_{h10}$ (Eq. (3)). However, in the coupled model, the values n_{mij} and n_{ij} can be zero or very small for some combined intervals of WS $_{max}$ and WDR $_{h10}$. Thus, it is impossible to produce a proper pdf of DR for all combinations of WS $_{max}$ and WDR $_{h10}$. In summary, the coupled model cannot produce a meaningful vulnerability tensor (V $_1$).

Similarly, the coupled model can also produce vulnerability matrices conditional on WDR_{h10} using Eq. (14).

$$V_3(m,j) = P(DR = dr_m | WDR_{h10} = wdr_j) = \frac{n_{mj}}{n_j}$$
 (14)

 n_{mj} = the number of data points of having the m-th DR interval, and j-th WDR_{h10} interval from vulnerability model. n_i = the number of data points of having the j-th

WDR_{h10} interval from vulnerability model.

Here again, for the coupled model, the values n_{mi} and n_i can be zero or very small for some intervals of WDR_{h10} and do not reflect the distribution p₂ of WS_{max} conditional on WDR_{h10} derived from the rain hazard model (Eq. (2)). Therefore, the coupled vulnerability matrix $V_3(m, j)$ is meaningless. As a result, the coupled vulnerability curve derived from $V_3(m,j)$, differs from the vulnerability curve from the decoupled model. Fig. 6 illustrates this situation by comparing the vulnerability curves conditional on WDR_{h10} from both the decoupled and coupled models for BC: open U6 S6 NSD IR C. The smooth decoupled vulnerability curve is derived from the complete pdf p₂ of WS_{max} conditional on WDR_{h10} derived from the hazard model (Eqs. (2) (6) and (8)). The coupled curve has oscillations for the reason described above and for large WDR_{h10} the rain hazard model only provides very few datapoints which results in large oscillations of DR. This last curve would lead to incorrect loss projections.

6.3 Insured losses

In the actuarial model, each building in an insurance portfolio is assigned a building class BC, with its corresponding vulnerability matrix V_2 and curve, and the combination of wind hazard intensity WS_{max} and vulnerability DR_{BC} results into mean insured loss $\$L_k$, for each property in a portfolio, given by Eq. (10). For the actuarial model there is no difference between the one-hazard and the coupled hazard-vulnerability approach. With the coupled vulnerability model, the actuarial model cannot take advantage of information on the secondary hazard WDR_{h10} at the location of the property.

7. Discussion

7.1 Computational efficiency of coupled vs. decoupled model

All things being equal in term of computer hardware (a desktop with Intel Core i7-10700KF CUP, 32 GB memory and 100 GB virtual memory), for one BC, the decoupled model required 38 minutes of computer time and 101 GB memory to run 1,476,000 simulations while the coupled model required 12 minutes of computer time and 45 GB memory to run 656,000 simulations. For 1500 BC's, that would result in 40 days of running time vs. 12.5 days for the decoupled and coupled models respectively. The coupled model computational efficiency is a factor of 3.2 improvement over the decoupled model. However, the coupled model produces only vulnerability matrices and curves conditional on WS_{max} as described previously. The computational efficiency of the decoupled model could be improved with more efficient source code, parallel computing, and more powerful computers. In terms of computer storage, the outputs of the decoupled model include the tensors V₁ with their vulnerability surfaces, and the vulnerability matrices V₂ and V₃ with their vulnerability curves, while the outputs of the coupled model include only

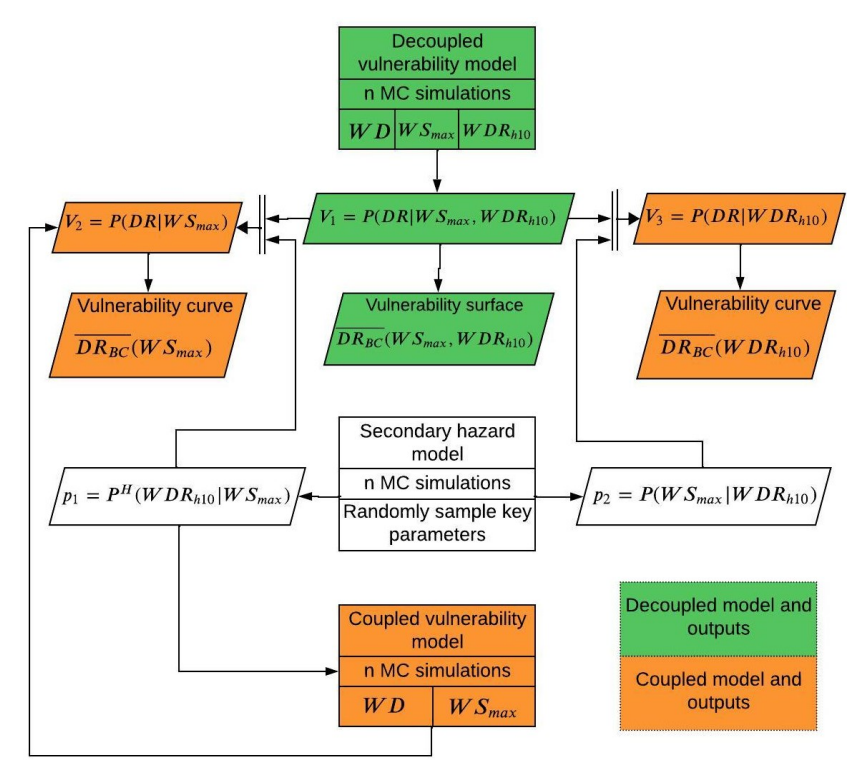


Fig. 7 Relationships between model outputs

the vulnerability matrices V₂ with their vulnerability curves, less than one third the needs of the decoupled model.

In the actuarial model which projects losses and recovery times, a simple test-case with 1,920,000 hypothetical buildings showed that a scenario analyses using vulnerability tensors and surfaces take twice the time of the same scenario analyses using vulnerability matrices and curves. Although the execution times of the scenarios are measured in seconds, for a stochastic analysis involving 50,000 scenarios, the overall difference in execution time could be significant. How significant would depend on the computer power available.

7.2 Relationship between model outputs

Fig. 7 shows the relationships between vulnerability models and secondary hazard model and where the coupling between the two can occur. In the figure, green boxes represent the stages where decoupling between the models exists, while orange represents where coupling occurs. The secondary hazard model, without any color in the figure, whether a standalone model or part of a multi-hazard model, yields the pdf's p_1 and p_2 from Eqs. (1) and (2).

In the case of the decoupled model, in a first stage (green in the figure), the MC simulations iterate over wind direction (WD), WS_{max} and WDR_{h10} , and result in a 3D vulnerability tensor, V_1 , completely independent of the hazard(s) model(s), which gives the probabilities of DR conditional on combinations of WS_{max} and WDR_{h10} . The graphical representation of V_1 is the vulnerability surface which gives the mean value of DR for each combination of WS_{max} and WDR_{h10} . In a second coupled stage (orange in the figure), the model converts V_1 into vulnerability

matrices, V_2 and V_3 , thought integration over p_1 and p_2 (section 4), which are embedded in this second stage of the model. V_2 and V_3 give the probabilities of DR conditional on either WS_{max} or WDR_{h10} . The graphical representation of V_2 and V_3 are vulnerability curves which give the mean values of DR for each value of WS_{max} or WDR_{h10} .

In the case of the coupled vulnerability model, the MC simulations iterate over WD and WS_{max} , whereas for each simulation WDR_{h10} is sampled from the pdf p_1 , which is embedded in the model, and the output is the same vulnerability matrix V_2 .

The actuarial model (not shown in the figure), shall need estimates of both WS_{max} and WDR_{h10} at property locations, from the primary and secondary hazard models, to be able to use V_1 to project losses. If only either WS_{max} or WDR_{h10} is available, then the actuarial model shall use V_2 or V_3 to predict losses.

7.3 Comparison between loss projections from the two approaches

It should be clear from the above that, for any BC, the main difference between the decoupled tensor V_1 (and its vulnerability surface) and the matrix V_2 (and its vulnerability curve) is that, for a given WS_{max} , there are many points on the vulnerability surface corresponding to all possible values of WDR_{h10} while there is only one point on the vulnerability curve corresponding the mean value of WDR_{h10} at that given WS_{max} .

Large insurance portfolios in general will have buildings belonging to multiple BC's. When doing a portfolio analysis, the projected losses at each property location, to which a BC is assigned, could vary widely depending on whether the loss was computed using a vulnerability surface or a vulnerability curve. It can be argued that the local projections from the vulnerability surface are more accurate since they use local rain hazard estimates instead of mean values. However, for large portfolios, if the number of properties belonging to each BC gets large enough at any WS_{max} (at least close to the number of simulations used for each WS_{max} in the coupled model) the law of large numbers plays out and the average of the results from the BC vulnerability surface at each WS_{max} shall converge to the WS_{max} results from the vulnerability curve. Tests show that for 2000 properties of the same BC the results of the two approaches converge with less than 2% difference. This is true of any BC, and hence for a heterogeneous portfolio, as long as they are represented in the portfolio by a large enough number of properties for each WS_{max} of interest, the aggregated portfolio losses from the two approaches shall be very similar.

For a small portfolio, this is not true. The local differences will not average out at the aggregated level, and large differences can be expected on the total portfolio losses, between the predictions based on vulnerability surfaces and curves. To summarize, in the case of smaller portfolios, a portfolio analysis based on a vulnerability surface, which can take advantage of the complete local hazard estimates shall be more accurate both at the local and at the aggregated level. In the case of a large portfolio, the analysis with vulnerability surface will still be more accurate at the property level, but both analyses will converge at the portfolio level.

8. Conclusions

This paper presents two approaches for multi-hazard vulnerability modeling, which are implemented into a component-based wind and rain hurricane vulnerability model, where the wind is the primary hazard and the rain is the secondary hazard. In the first approach, in a decoupled first tier, the primary and secondary hazard models and vulnerability model are independent of each other, and the primary output is a vulnerability tensor (V₁) conditional upon both hazard intensities. The decoupling facilitates the testing of the influence of different hazard models on the outputs of the actuarial model. In a second coupled tier, this approach has the unique advantage that it can also produce vulnerability matrices (V2 or V3) conditional on either the primary or the secondary hazard, although the independence of hazard and vulnerability model is lost, since in each case the vulnerability matrix results from the integration of the tensor V₁ over the pdf of one of the hazard conditional on the other. In the purely coupled second approach, where the secondary hazard model is embedded in the MC simulations of the vulnerability model, the only outputs of the vulnerability model are vulnerability matrices (V₂) conditional on the primary hazard. The graphic representations of V_1 , V_2 , and V_3 are vulnerability surfaces and vulnerability curves.

The paper shows the pros and cons of each approach. For sufficiently large portfolios where all the building

classes have large populations in each wind speed interval of interest, there are no statistical differences between the results of the two approaches at the aggregated level of portfolio losses. The decoupled approach though, which takes advantage of all the local hazard information, produces more realistic loss projections for each individual portfolio property. The decoupled approach has also the distinct advantage of being the only approach which can produce vulnerability matrices and curves conditional on the secondary hazard, which can be very useful for loss estimations and mitigation studies. For smaller portfolios or portfolios where certain building classes might be underrepresented, there can be significant differences between the loss projections from the decoupled model (based on vulnerability surfaces and local hazard estimates) and coupled model (based on vulnerability curves and mean values of secondary hazard), with the decoupled model providing more realistic results.

In terms of computational efficiency, the generation of the vulnerability matrices and curves from the coupled approach could be 3 to 4 times faster than the generation of the vulnerability tensors and surfaces, and subsequent matrices and curves from the decoupled approach, and require less storage space. At the actuarial level, the execution time of a stochastic portfolio analysis could be twice as long using a library of decoupled vulnerability tensors than using a library of vulnerability matrices. The significance of the extra computer time will depend on the computing power available.

In practice, many hazard models might provide local primary hazard intensities only, in which case, the only option for the cat model is to project losses and recovery times based on the vulnerability matrices from the second coupled tier of the first approach or from the purely coupled second approach. Hopefully, this research shall raise awareness of the issues linked to coupled models, and the constant advances in computer power might improve the computational efficiency and attractiveness of the decoupled approach. Validation is an important issue as well, since proper validation of a cat model using a decoupling approach between hazard and vulnerability requires both primary and secondary hazard data at each insurance claim location.

Acknowledgments

The National Science Foundation supports the Center for Wind Hazard and Infrastructure Performance (WHIP-C) through grant # 1841523, and the Industrial Advisory Board of the WHIP-C supported this work through grant number WHIP2020_06. The Florida Office of Insurance Regulation (FOIR) also supported part of this work. The opinions, findings, and conclusions presented in this paper are those of the author alone, and do not necessarily represent the views of the NSF or the WHIP-C or the FOIR.

References

- Baradaranshoraka, M., Pinelli, J.-P., Gurley, K., Peng, X. and Zhao, M. (2017), "Hurricane Wind versus Storm Surge Damage in the Context of a Risk Prediction Model", *J. Struct. Eng.*, **143**(9). https://doi.org/10.1061/(asce)st.1943-541x.0001824.
- Baradaranshoraka, M., Pinelli, J.-P., Gurley, K., Zhao, M., Peng, X. and Paleo-Torres, A. (2019), "Characterization of coastal flood damage states for residential buildings", *ASCE-ASME J. Risk Uncertainty Eng. Sys. Part A: Civil Eng.*, **5**(1). https://doi.org/10.1061/ajrua6.0001006.
- Barbato, M., Petrini, F., Unnikrishnan, V.U. and Ciampoli, M. (2013), "Performance-Based Hurricane Engineering (PBHE) framework", *Struct. Safety*, **45**, 24-35. https://doi.org/10.1016/J.STRUSAFE.2013.07.002.
- Bhandari, A., Datta, G. and Bhattacharjya, S. (2018), "Efficient wind fragility analysis of RC high rise building through metamodeling", *Wind Struct.*, **27**(3), 199-211. https://doi.org/10.12989/was.2018.27.3.199.
- Biasi, G., Mohammed, M.S. and Sanders, D.H. (2017), "Earthquake damage estimations: ShakeCast case study on Nevada bridges", *Earthq. Spectra*, **33**(1), 45-62. https://doi.org/10.1193/121815EQS185M.
- Borgonovo, E., Castaings, W. and Tarantola, S. (2012), "Model emulation and moment-independent sensitivity analysis: An application to environmental modelling", *Environ. Modelling Softw.*, **34**, 105-115. https://doi.org/10.1016/J.ENVSOFT.2011.06.006.
- Chian, S.C. (2016), "A complementary engineering-based building damage estimation for earthquakes in catastrophe modeling", *Int. J. Disaster Risk Sci.*, 7(1), 88-107. https://doi.org/10.1007/S13753-016-0078-5/TABLES/10.
- Ciabattoni, M., Petrini, F. and Pampanin, S. (2024), "Multi-hazard design of low-damage high-rise steel-timber buildings subjected to wind and earthquake loading", *Eng. Struct.*, **303**, 117522. https://doi.org/10.1016/J.ENGSTRUCT.2024.117522.
- Dietrich, J.C., Tanaka, S., Westerink, J.J., Dawson, C.N., Luettich, R.A., Zijlema, M., Holthuijsen, L.H., Smith, J.M., Westerink, L. G. and Westerink, H.J. (2012), "Performance of the unstructured-mesh, SWAN+ ADCIRC model in computing hurricane waves and surge", *J. Sci. Comput.*, **52**(2), 468-497. https://doi.org/10.1007/S10915-011-9555-6/METRICS.
- Dong, W. (2002), "Engineering models for catastrophe risk and their application to insurance", *Earthq. Eng. Eng. Vib.*, **1**, 145-151. https://doi.org/https://doi.org/10.1007/s11803-002-0018-9.
- FPHLM. (2023), Florida Public Hurricane Loss Model technical document.
- https://fchlpm.sbafla.com/media/ghll1ufp/2023_03_11_fphlm_2 022 submission document-1.pdf.
- Francioli, M., Petrini, F. and Bontempi, F. (2023), "Structural robustness analysis of RC frames under seismic and blast chained loads scenarios", *J. Build. Eng.*, **67**, 105970. https://doi.org/10.1016/J.JOBE.2023.105970.
- Geist, E.L., Lynett, P.J. and Chaytor, J.D. (2009), "Hydrodynamic modeling of tsunamis from the Currituck landslide", *Marine Geology*, **264**(1-2), 41-52. https://doi.org/10.1016/J.MARGEO.2008.09.005.
- Hamid, S.S., Pinelli, J.P., Chen, S.C. and Gurley, K. (2011), "Catastrophe model-based assessment of hurricane risk and estimates of potential insured losses for the State of Florida", *Nat. Haz. Rev.*, **12**(4), 171-176. https://doi.org/10.1061/(ASCE)NH.1527-6996.0000050.
- Hatzikyriakou, A. and Lin, N. (2016), "Impact of performance interdependencies on structural vulnerability: A systems perspective of storm surge risk to coastal residential communities", *Reliability Eng. Syst. Safety*, **158**, 106-116. https://doi.org/10.1016/j.ress.2016.10.011.

- Henderson, D.J. and Ginger, J.D. (2007), "Vulnerability model of an Australian high-set house subjected to cyclonic wind loading", *Wind Struct.*, **10**(3), 269-286. https://doi.org/10.12989/was.2007.10.3.269.
- Holland, G.J. (1980), "An analytic model of the wind and pressure profiles in hurricanes", *Month. Weather Rev.*, **108**(8), 1212-1218. http://danida.vnu.edu.vn/cpis/files/Refs/TCs/0-An%20Analytic%20Model%20of%20the%20Wind%20and%20 Pressure%20Profiles%20in%20Hurricanes%20Holland(1980).pdf
- Johnson, T., Pinelli, J.-P., Baheru, T., Chowdhury, A.G., Weekes, J. and Gurley, K. (2018), "Simulation of rain penetration and associated damage in buildings within a hurricane vulnerability model", *Nat. Haz. Rev.*, **19**(2), 04018004. https://doi.org/10.1061/(ASCE)NH.1527-6996.0000288.
- Kennedy, A., Copp, A., Florence, M., Gradel, A., Gurley, K., Janssen, M., Kaihatu, J., Krafft, D., Lynett, P., Owensby, M., Pinelli, J.-P., Prevatt, D. O., Rogers, S., Roueche, D. and Silver, Z. (2020), "Hurricane Michael in the area of Mexico beach, Florida", *J. Waterway, Port, Coastal, Ocean Eng.*, **146**(5). https://doi.org/10.1061/(asce)ww.1943-5460.0000590.
- Knabb, R.D., Brown, D.P. and Rhome, J.R. (2006), *Tropical Cyclone Report Hurricane Rita*. https://www.nhc.noaa.gov/data/tcr/AL182005 Rita.pdf.
- Knabb, R.D., Rhome, J.R. and Brown, D.P. (2005), *Tropical Cyclone Report Hurricane Katrina*. https://www.nhc.noaa.gov/data/tcr/AL122005 Katrina.pdf.
- Li, Y., Ahuja, A. and Padgett, J.E. (2012), "Review of methods to assess, design for, and mitigate multiple hazards", *J. Perform. Construct. Facilities*, **26**(1), 104-117. https://doi.org/10.1061/(ASCE)CF.1943-5509.0000279/ASSET/FC216328-D77D-4CA5-9D36-394E19F7EEA9/ASSETS/IMAGES/LARGE/9.JPG.
- Lu, Y., Zhang, L., He, Z., Feng, F. and Pan, F. (2021), "Wind-induced vibration fragility of outer-attached tower crane to super-tall buildings: A case study", *Wind Struct.*, **32**(5), 405-421. https://doi.org/10.12989/WAS.2021.32.5.405.
- Luger, S.A. and Harris, R.L. (2010), "Modelling Tsunamis generated by earthquakes and submarine slumps using Mike 21", *International MIKE by DHI Conference 2010*. https://www.dhigroup.com/upload/publications/mike21/Luger_2 010.pdf.
- Ma, L., Christou, V. and Bocchini, P. (2021), "Framework for probabilistic simulation of power transmission network performance under hurricanes", *Reliability Eng. Syst. Safety*, 217, 108072. https://doi.org/10.1016/j.ress.2021.108072.
- Mahmoudi, A., Nasrollahzadeh, K. and Jafari, M.A. (2021), "Probabilistic failure analysis of 400 kV transmission tower-line system subjected to wind and ice hazards", *Wind Struct.*, **33**(3), 251-264. https://doi.org/10.12989/was.2021.33.3.251.
- Marks, F.D., Atlas, D. and Wills, P.T. (1993), "Probability-matched reflectivity-rainfall relations for a hurricane from aircraft observations", *J. Appl. Meteorol. Climatol.*, **32**(6), 1134-1141. https://doi.org/https://doi.org/10.1175/1520-0450(1993)032<1134:PMRRRF>2.0.CO;2.
- Matyas, C.J. (2010), "Associations between the size of hurricane rain fields at landfall and their surrounding environments", *Meteorol. Atmos. Phys.*, **106**(3-4), 135-148. https://doi.org/10.1007/s00703-009-0056-1.
- Michel-Kerjan, E., Hochrainer-Stigler, S., Kunreuther, H., Linnerooth-Bayer, J., Mechler, R., Muir-Wood, R., Ranger, N., Vaziri, P. and Young, M. (2013), "Catastrophe risk models for evaluating disaster risk reduction investments in developing countries", *Risk Anal.*, 33(6). https://doi.org/10.1111/j.1539-6924.2012.01928.x.
- Miller, B. (2018), 2017 was the costliest year for weatherl disasters by a long shot | CNN.

- https://www.cnn.com/2018/01/08/us/2017-costliest-disasters/index.html.
- Ming, X., Xu, W., Li, Y., Du, J., Liu, B. and Shi, P. (2015), "Quantitative multi-hazard risk assessment with vulnerability surface and hazard joint return period", *Stochastic Environ. Research Risk Assessment*, 29(1), 35-44. https://doi.org/10.1007/S00477-014-0935-Y/FIGURES/4.
- NOAA. (2023), Billion-Dollar Weather and Climate Disasters. https://www.ncei.noaa.gov/access/billions/.
- Nofal, O.M. and Lindt, J. W. van de. (2020), "Probabilistic Flood Loss Assessment at the Community Scale: Case Study of 2016 Flooding in Lumberton, North Carolina", ASCE-ASME J. Risk Uncertainty Eng. Syst. Part A: Civil Eng., 6(2), 05020001. https://doi.org/10.1061/AJRUA6.0001060.
- Nofal, O.M., van de Lindt, J.W., Do, T.Q., Yan, G., Hamideh, S., Cox, D.T. and Dietrich, J.C. (2021), "Methodology for regional multihazard hurricane damage and risk assessment", *J. Struct. Eng.*, 147(11). https://doi.org/10.1061/(asce)st.1943-541x.0003144.
- Paleo-Torres, A., Gurley, K., Pinelli, J.P., Baradaranshoraka, M., Zhao, M., Suppasri, A. and Peng, X. (2020), "Vulnerability of Florida residential structures to hurricane induced coastal flood", Eng. Struct., 220, 111004. https://doi.org/10.1016/J.ENGSTRUCT.2020.111004.
- Petrini, F., Gkoumas, K., Rossi, C. and Bontempi, F. (2020), "Multi-hazard assessment of bridges in case of hazard chain: State of play and application to vehicle-pier collision followed by fire", *Front. Built Environ.*, **6**, 580854. https://doi.org/10.3389/FBUIL.2020.580854/BIBTEX.
- Pinelli, J.-P., Pita, G., Gurley, K., Torkian, B., Hamid, S. and Subramanian, C. (2011), "Damage characterization: Application to Florida Public Hurricane Loss Model", *Nat. Haz. Rev.*, 12(4), 190-195. https://doi.org/10.1061/(ASCE)NH.1527-6996.0000051.
- Pita, G., Pinelli, J.-P., Cocke, S., Gurley, K., Mitrani-Reiser, J., Weekes, J. and Hamid, S. (2012), "Assessment of hurricaneinduced internal damage to low-rise buildings in the Florida Public Hurricane Loss Model", J. Wind Eng. Ind. Aerod., 104, 76-87. https://doi.org/10.1016/j.jweia.2012.03.023
- Pita, G., Pinelli, J.-P., Gurley, K. and Mitrani-Reiser, J. (2015), "State of the art of hurricane vulnerability estimation methods: A review", *Nat. Haz. Rev.*, **16**(2), 04014022. https://doi.org/10.1061/(ASCE)NH.1527-6996.0000153.
- Pita, G.L., Pinelli, J.P., Gurley, K., Weekes, J., Cocke, S. and Hamid, S. (2016), "Hurricane vulnerability model for mid/highrise residential buildings", *Wind Struct.*, **23**(5), 449-464. https://doi.org/10.12989/WAS.2016.23.5.449.
- Pita, G.L., Pinelli, J.P., Gurley, K.R. and Hamid, S. (2013), "Hurricane vulnerability modeling: Development and future trends", *J. Wind Eng. Ind. Aerod.*, **114**, 96-105. https://doi.org/10.1016/J.JWEIA.2012.12.004.
- Powell, M., Soukup, G., Cocke, S., Gulati, S., Morisseau-Leroy, N., Hamid, S., Dorst, N. and Axe, L. (2005), "State of Florida hurricane loss projection model: Atmospheric science component", *J. Wind Eng. Ind. Aerod.*, **93**(8), 651-674. https://doi.org/10.1016/J.JWEIA.2005.05.008.
- Powell, M.D., Murillo, S., Dodge, P., Uhlhorn, E., Gamache, J., Cardone, V., Cox, A., Otero, S., Carrasco, N., Annane, B. and Fleur, R.S. (2010), "Reconstruction of Hurricane Katrina's wind fields for storm surge and wave hindcasting", *Ocean Eng.*, 37(1), 26-36. https://doi.org/10.1016/J.OCEANENG.2009.08.014.
- RMS (Risk Management Solutions). (2021), North Atlantic Hurricane Models. http://www.rms.com/.
- Sim, V., Jung, W., Sim, V. and Jung, W. (2020), "Wind-induced fragility assessment of protruding sign structures", *Wind Struct.*, **31**(5), 381. https://doi.org/10.12989/WAS.2020.31.5.381.

- Smith, A.B. (2023), 2022 U.S. billion-dollar weather and climate disasters in historical context | NOAA Climate.gov. https://www.climate.gov/news-features/blogs/2022-us-billion-dollar-weather-and-climate-disasters-historical-context.
- Tilloy, A., Malamud, B.D., Winter, H. and Joly-Laugel, A. (2019), "A review of quantification methodologies for multi-hazard interrelationships", *Earth-Sci. Rev.*, **196**, 102881 https://doi.org/10.1016/j.earscirev.2019.102881.
- Tomiczek, T., Kennedy, A. and Rogers, S. (2014), "Collapse limit state fragilities of wood-framed residences from storm surge and waves during hurricane Ike", *J. Waterway, Port, Coastal, Ocean Eng.*, 140(1), 43-55. https://doi.org/10.1061/(ASCE)WW.1943-5460.0000212/ASSET/466D5D99-F32C-4AB2-BDAA-B1584B2C2627/ASSETS/JMAGES/LABGE/FIGUIDE12 IDG
 - B1584B2C2627/ASSETS/IMAGES/LARGE/FIGURE12.JPG.
- Wang, D., Li, S., Sun, C., Huang, G. and Yang, Q. (2021), "Assessment of wind-induced fragility of transmission towers under quasi-static wind load", *Wind Struct.*, **33**(4), 343-352. https://doi.org/10.12989/was.2021.33.4.343.
- Wei, Z., Pinelli, J.-P. and Gurley, K. (2024), "Component-based hurricane vulnerability model for mid/high-rise commercial residential buildings", *Int. J. Dis. Risk Reduction*, **100**, 104222. https://doi.org/10.1016/j.ijdrr.2023.104222.
- Wei, Z., Pinelli, J.-P., Gurley, K., Hamid, S. and Flannery, G. (2024), "Component-based estimation of recovery time and time-related expenses after hurricane events", *Front. Built Environ.*, **9**, 1295619. https://doi.org/10.3389/fbuil.2023.1295619.
- Zaghi, A.E., Padgett, J.E., Bruneau, M., Barbato, M., Li, Y., Mitrani-Reiser, J. and McBride, A. (2016), "Establishing common nomenclature, characterizing the problem, and identifying future opportunities in multihazard design", *J. Struct. Eng.*, 142(12), H2516001. https://doi.org/10.1061/(ASCE)ST.1943-541X.0001586/ASSET/FE098C96-6A53-42CB-802B-1BBFC0157F6B/ASSETS/IMAGES/LARGE/FIGURE2.JPG.

FR